J Solid State Electrochem (2010) 14:57–62
DOI 10.1007/s10008-009-0788-3

ORIGINAL PAPER

Electrocrystallization of palladium from $Pd(NH_3)_4Cl_2$ bath on stainless steel 316L

I. Danaee · F. Shoghi · M. Dehghani Mobarake · M. Kameli

Received: 13 September 2008 / Revised: 12 December 2008 / Accepted: 10 January 2009 / Published online: 25 January 2009

Abstract Electrochemical deposition of palladium from 0.04 M $Pd(NH_3)_4Cl_2$, NH_4Cl, and NH_4OH bath (pH=10) on stainless steel electrode was studied by voltammetry, chronopotentiometry, and chronoamperometry. Crossovers in cyclic voltammograms demonstrate that the deposition of palladium proceed via a nucleation/growth mechanism. Chronopotentiograms indicate that palladium reduction is not controlled by diffusion and Sand's law is not obeyed. In the early stage of the deposition, two-dimensional (2D) nucleation and growth proceeding through instantaneous and a multitude of progressive steps followed the initial double layer charging. The processes are manifested as broad maxima in chronoamperogram and after which the current transient terminates to a plateau. Non-linear fitting methods were applied to obtain the kinetic parameters in the light of Bewick, Fleischmann, and Thirsk theory for 2D and Armstrong, Fleischmann, and Thirsk model for 3D nucleation and growth process.

Keywords Current transient · Electrocrystallization · Nucleation · Growth · Palladium

I. Danaee (✉)
Department of Chemistry, K. N. Toosi University of Technology,
P. O. Box 15875-4416, Tehran, Iran
e-mail: danaee@dena.kntu.ac.ir

F. Shoghi · M. Kameli
Inhibitors Chemical & Petrochemical Division,
Research Institute of Petroleum Industry (RIPI),
P. O. Box 14665-199, Tehran, Iran

M. Dehghani Mobarake
Catalysis Research Center, Kinetics & Reaction Engineering,
Research Institute of Petroleum Industry (RIPI),
P. O. Box 14665-1998, Tehran, Iran

Introduction

The electrocrystallization of metal on various substrates continues to provoke a great deal of interest in modern electrochemistry due to its technological importance [1]. Nucleation kinetics and the growth of the first metallic nuclei formed on a substrate are critical steps that determine the physicochemical properties of electrodeposits and their studies are crucial in the understanding and control of the processes [2–6]. This early stage of electrochemical phase transformation is usually associated with a one-, two-, or three-dimensional nucleation process [7–10]. In this respect, the classical vapor phase nucleation theory [11, 12], which has been extended to electrochemical deposition, is relatively simple and requires the definition of dimensionless supersaturation parameters, S, in terms of the overpotential, That is,

$$S = \frac{zF\eta}{RT} \tag{1}$$

The nucleation rate is then represented by

$$J = A\exp\left(-\frac{B}{\eta}\right) \tag{2}$$

where B is a parameter that contains several constant terms [12].

According to this equation, a critical overpotential (corresponding to a critical supersaturation in the homogeneous phase theory) must be reached before the onset of nucleation. Both the metal ion and the substrate material control this critical overpotential. During the nucleation study, it is observed that the nuclei are randomly distributed crystallites of nearly identical size and growing under mass transfer control [7, 9]. Rising current transients are observed in a chronoamperometric run which reflect the increase in current

as each nucleus grows in size and is accompanied by a rise of the total area of electroactive surface. Well before the overlap of the diffusion zones of adjacent nuclei, the total current $I_{N,t}$ can be expressed by the sum of the contribution $I_{i,t}$ of individual nuclei [9].

$$I_{N,t} = \sum I_{i,t} \tag{3}$$

Furthermore, when the nucleation process takes place, one-, two-, or three-dimensional morphologies can be observed for the growth of nuclei on suitable nucleation sites. Whatever the growth morphology, two different regimes can be established. In the first one, the rate-determining step is represented by the metal incorporation into the growth site whilst for the second one the rate-determining step is the mass transfer of the depositing metal ions towards the surface of the growing nucleus [9].

Palladium has excellent physical and chemical properties such as corrosion and wear resistance, thermal stability, and high catalytic activity for various chemical reactions, so that it is mainly used for industrial applications like catalysis and electrical devices [13–14]. Palladium thin films deposited on gold and platinum substrates demonstrate extremely high catalytic activities in the electrooxidation reaction of small organic molecules such as formaldehyde and formic acid [15–19]. The electrodeposition of palladium has been studied on various electrodes such as graphite, polymer matrix, and porous stainless steel electrode [20–25]. The electrochemical layer-by-layer growth of the palladium was reported on copper and a gold single crystal electrode [26–28]. Electrodeposition of metal on steel substrate has received some attention by several authors [29–31]. Steel modified with metal and alloy has been used for electrocatalytic reaction due to low cost and good conductivity [32–34].

The purpose of the present work is to determine the kinetics and mechanism of the electrodeposition of palladium from 0.04 M $Pd(NH_3)_4Cl_2$, NH_4Cl, and NH_4OH on a stainless steel substrate where electrochemical methods have been employed.

Experimental

Materials used in this work were analytical grade of Merck origin. The experiments were carried out at 25 °C in a conventional three-electrode cell. The working electrode was a steel 316L rod mounted in Teflon with an apparent exposed area of 0.25 cm^2. Its potential was monitored against an Ag–AgCl reference electrode. A large graphite rod was used as the counter electrode.

Prior to each experiment, the surface pretreatment of working electrode was performed by hand polishing of the electrode surface with successive grades of emery papers down to 3000 grit up to a mirror finish. The polished electrode was then degreased with acetone and washed with running, doubly distilled water.

The electrochemical cell was powered by EG&G model 273A potentiostat/galvanostat runs by a PC through M270 software. The methods of cyclic voltammetry, chronopotentiometry, and chronoamperometry have been employed. Electrochemical data from the current transient study were evaluated quantitatively using a home-made software package developed for personal computers.

Result and discussion

Cyclic voltammogram obtained in the potential range of 0.2 to −1.5 V/Ag–AgCl with a scan rate of 50 mV s^{-1} is presented in Fig. 1a. During the scan in the cathodic direction, significant crystallization overpotential can be noticed before palladium electrodeposition occurs; the cathodic current density increases at potential more negative than −0.77 V. The reduction peak is observed at −1.35 V and, at more negative potential, current density increases again due to the hydrogen evolution. Also, Pd is known to be an excellent hydrogen absorber [35]. Therefore, hydrogen absorption occurred in thin film of palladium at this potential range. The reverse scan shows initially a decrease in current density, and two crossovers are observed, one at more negative than crystallization potential and the other at zero current, characteristic of metal deposition onto substrates of different nature. From Fig. 1, equilibrium potential of the system can be obtained −0.57 V/Ag–AgCl. On reversing the scan direction, metal already deposited on the electrode surface continues to grow as a result of the $Pd^{2+} + 2e \rightleftarrows Pd$ reaction remaining thermodynamically and kinetically favorable. In the following reverse scan, at more

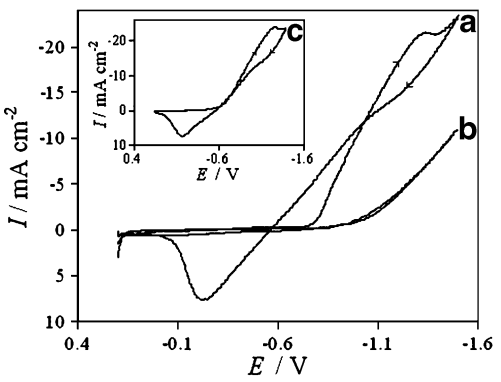

Fig. 1 **a** First cycle of voltammogram of the palladium electrodeposition from 0.04 M $Pd(NH_3)_4Cl_2$, NH_4Cl, and NH_4OH bath. The scan began at 0.2 V/Ag–AgCl with a scan rate of 50 mV s^{-1}. **b** Cyclic voltammogram of stainless steel electrode in NH_4Cl and NH_4OH bath with a scan rate of 50 mV s^{-1}. **c** Fifth cycle of voltammogram of the palladium electrodeposition with a scan rate of 50 mV s^{-1}

positive potential, an anodic peak appears which is associated with the stripping of Pd formed during the scan in negative direction. The relative location of the deposition and stripping signals suggest complex irreversible type identified by Fletcher [36, 37]. The cyclic voltammetry measurement with the steel electrode immersed in an aqueous solution containing solely the supporting electrolyte is also shown in Fig. 1b. As can be seen in the cathodic scan, hydrogen evolution reaction is stated in more negative potential and no increasing current is observed due to electrodeposition.

Integration of both cathodic and anodic peaks gave a charge ratio $Q_c/Q_a>1$. This behavior was already observed in other systems [38] and explained in terms of a residual metal deposit on the electrode surface. This excess of cathodic charge is also due to H_2 evolution. After further cycling, lower crystallization overpotential is needed before palladium electrodeposition occurs (Fig. 1c). This indicates that residual palladium deposit after each scan promotes the nucleation and deposition of palladium in the following cathodic cycle.

When cathodic limit of scan is located at the foot of the reduction peak (Fig. 2), there is also a small peak more positive than the main deposition process corresponding to the formation of surface layer; also, a crossover loop signifying nucleation/growth in the course of the anodic scan is observed [39, 40]. Since the activity of the palladium metal is not fixed before the main deposition process, it is possible that underpotential deposition can occur. The charge, Q, under this peak is approximately 3×10^{-4} C cm^{-2}, which is assumed that the small peak corresponds to the underpotential deposition of palladium and, according to Faraday's law, can account for about 1/2 of a monolayer. In this case, it was found that the crossover potential is independent on the negative reverse potential at the considered concentrations. From these and the Fletcher

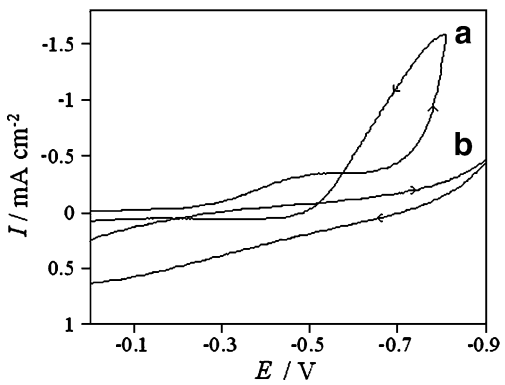

Fig. 2 **a** Cyclic voltammogram of the stainless steel electrode in limited potential range due to monolayer formation. The scan began at 0.2 V/Ag–AgCl with a scan rate of 50 mV s^{-1}. **b** Cyclic voltammogram of stainless steel electrode in NH_4Cl and NH_4OH bath with a scan rate of 50 mV s^{-1}

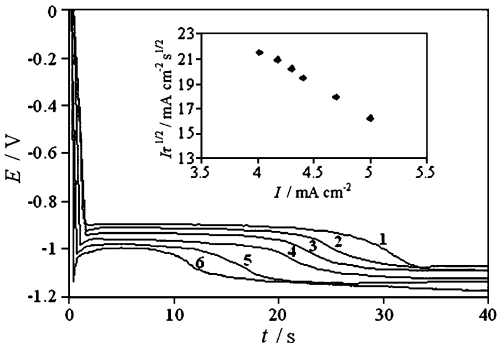

Fig. 3 Chronopotentiogram of the palladium electrodeposition from 0.04 M $Pd(NH_3)_4Cl_2$, NH_4Cl, and NH_4OH bath at different current densities: I_1=4, I_2=4.2, I_3=4.3, I_4=4.4, I_5=4.7, and I_6=5 mA cm^{-2}

[36, 37] theory, it is concluded that the growth rate is independent on the nucleation time (the experimental range of time selected for examining the growth of the nuclei). Therefore, the nuclei growth rate is controlled by charge transfer and is determined only by the imposed potential.

The current step method is also a useful means of detecting the presence of nucleation. Potential maxima at the beginning of the time of experimental curve, transition time, can be attributed to the nucleation process [41]. Experimental chronopotentiograms exhibit a characteristic maximum in the early stages of deposition as shown in Fig. 3. At the very beginning of the chronopotentiogram, the steep falling potential has contributions of both double layer as well as pseudo capacitor charging [42] of adsorption followed by monolayer deposition of the electroactive constituents. As the potential increases, nucleation takes place [43] and an overvoltage is required to meet the galvanostatic conditions. As soon as nuclei are growing, the overvoltage for reduction decreases. The product $I\tau^{1/2}$ was found to decrease with increasing applied current density, I, showing that the deposition of palladium is not controlled by diffusion and the reaction appears to be confined to the surface or near surface domains [44].

In order to gain information about the kinetics of electrocrystallization of palladium, chronoamperometric studies were made at different step cathodic potentials (Fig. 4). The effect of step cathodic potentials (in the range of −0.79 to −0.84 V) on the current–time transients in solution containing 0.04 M $Pd(NH_3)_4Cl_2$, NH_4Cl, and NH_4OH at 25 °C were studied. Rising current was observed after the initial decline of current. Analysis of time dependence of rising portion prior to broad maxima indicates nucleation step leading to a new phase formation and growth [45]. At the beginning of each transient, there is inevitably a charging current that decays sharply during the processes of nucleation and growth of a palladium film on the surface. During this stage of the growth of the film, the nuclei develop diffusion zones around themselves. As these zones

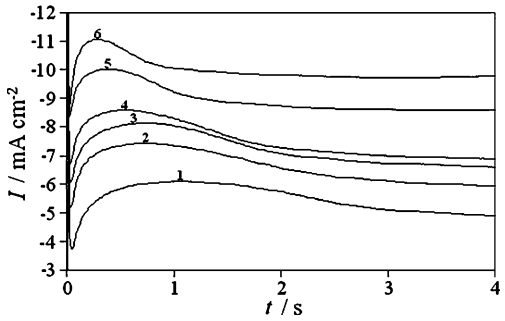

Fig. 4 Potentiostatic current transient obtained for deposition of Pd on stainless steel at different potentials: *1* −0.79, *2* −0.8, *3* −0.81, *4* −0.82, *5* −0.83, and *6* −0.84 V/Ag–AgCl. Initial potential used in current transients is −0.1 V/Ag–AgCl

overlap, the current should decrease due to the linear diffusion of the electroactive ions towards a planar electrode but nucleation and growth of a new layer on the underlying monolayer prevent a drop in current. Therefore, broad maxima created in the current transient and after maxima current transient were terminated to a plateau. The value of current density increases slightly with increasing applied potential.

Considering the broad maxima observed in the amperograms in the course of the growth of palladium films, a suitable model for the nucleation and growth processes of palladium seems to be the overlapping of two growth steps. The first step is layer-by-layer growth on the basis of the theory developed by Bewick, Fleishmann, and Thirsk [46]. The theory models a two-dimensional growth determined by the incorporation of adatoms to the periphery of a growing nucleus and also takes into account the overlap of the growing nuclei. In the content of this theory, two distinct types of nucleation, instantaneous and progressive, are distinguished. The current–time dependencies of the two types are distinctly different and follow Eqs. (4) and (5)

$$I_{2\mathrm{DI}} = \frac{2\pi nFMhN_0k^2t}{\rho}\exp\left[-\frac{\pi N_0M^2k^2\,t^2}{\rho^2}\right] \tag{4}$$

$$I_{2DP} = \frac{n\pi FMhAN_0k^2t^2}{\rho}\exp\left[-\frac{\pi M^2AN_0k^2\,t^3}{3\rho^2}\right] \tag{5}$$

These equations predict a maximum in the current–time curve for instantaneous with

$$t_m = \left(\frac{\rho^2}{2\pi N_0M^2k}\right)^{1/2} \tag{6}$$

$$I_{\mathrm{m}} = nFhk(2\pi N_0)^{1/2}\exp\left(-\frac{1}{2}\right) \tag{7}$$

and through Eqs. (8) and (9) for the progressive process.

$$t_m = \left(\frac{2\rho^2}{\pi M^2AN_0k}\right)^{1/3} \tag{8}$$

$$I_{\mathrm{m}} = nF\left(\frac{4\pi AN_0k\rho}{M}\right)^{1/3}h\exp\left(-\frac{2}{3}\right) \tag{9}$$

The follow-up step of growth has been put forward by the theory developed by Armstrong, Fleischmann, and Thirsk (AFT) [47]. This model assumes a three-dimensional (3D) nucleation limited by the incorporation of adatoms into the lattice and takes into account the overlapping of growing nuclei having the right circular cone geometry. The AFT growth model leads to a plateau at longer time in Fig. 4. According to this model, the current–time dependency of a progressive nucleation process follows

$$I_{3\mathrm{DP}} = nFk_{2\mathrm{g}}\left[1-\exp\left[-\frac{\pi M^2A_{\mathrm{g}}N_{0\mathrm{g}}\,k_{1\mathrm{g}}^2\,t^3}{3\rho^2}\right]\right] \tag{10}$$

With the value of the steady state current is given by

$$I_m = \frac{nFk_{2\mathrm{g}}}{4} \tag{11}$$

In the above equations N_0 is the number density of active sites, k is the lateral growth rate constant of nuclei, A is the nucleation rate constant, M is the molecular weight, ρ is the density of the deposited material, h is the thickness of the deposited layer, $k_{1\mathrm{g}}$ and $k_{2\mathrm{g}}$ are the rate constants for parallel and perpendicular growth with respect to the electrode surface, and nF refers to the molar charge transferred during electrodeposition.

The entire process can be described in terms of the contribution of every step, namely:

$$I = I_{\mathrm{DL}} + I_{2\mathrm{DI}} + I_{2\mathrm{DP}} + I_{2\mathrm{DP}} + I_{3\mathrm{DP}} \tag{12}$$

And in more detail

$$\begin{aligned} I = {} & k_{\mathrm{D1}}\exp\left(-k_{\mathrm{D2}}t\right) + \frac{2\pi nFMh_1N_{01}k_1^2t}{\rho}\exp\left(-\frac{\pi N_{01}M^2k_1^2t^2}{\rho^2}\right) \\ & + \frac{\pi nFMh_2A_1N_{02}k_2t^2}{\rho}\exp\left(-\frac{\pi M^2A_1N_{02}k_2^2t^3}{3\rho^2}\right) \\ & + \frac{\pi nFMh_3A_2N_{03}k_3t^2}{\rho}\exp\left(-\frac{\pi M^2A_2N_{03}k_3^2t^3}{3\rho^2}\right) \\ & + nFk_{2\mathrm{g}}\left[1-\exp\left[-\frac{\pi M^2AN_{0\mathrm{g}}k_{1\mathrm{g}}^2t^3}{3\rho^2}\right]\right] \end{aligned} \tag{13}$$

The first term in the left-hand side is due to double layer charging while the third, fourth, … terms are related to the contributions of progressive nucleation on sites with $A_iN_{0i}k_i^2$, i=1, 2,…, characteristics. Figure 5a and b presents a theoretically derived current transient at −0.79 and −0.84 V/Ag–AgCl that perfectly fits the experimental findings. It also presents the contributions from the double layer and several nucleation processes. In the applied

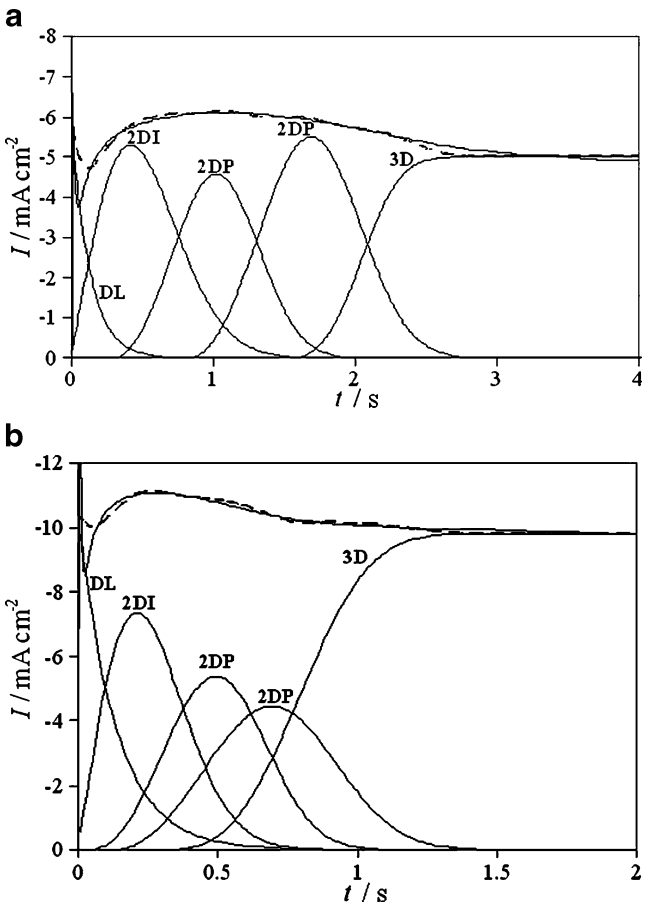

Fig. 5 Experimental current transient (—) recorded at **a** −0.79 and **b** −0.84 V/Ag–AgCl and a corresponding theoretical curve (- - -). Contributions to the transient current from the double layer charging phenomenon (I_{DL}) and consecutive 2D and 3D growth process are shown separately

potential range (Fig. 5a, b), strong overlapping of the processes is distinct. 2DI process strongly overlaps with double layer charging in the beginning and merges to 2DP nucleation as it terminates. Also, 3D process starts to grow prior to the completion of 2D layers. The overlapping actually puts the entire process into the natural course and without its contribution no good fit between the experimental and theoretical results is envisaged. In fact, the classical 2D–2D model of Frank–van der Merwe that follows a layer-by-layer approach [48] can hardly account for our findings. Also, the model of 3D island growth on top of predeposited monolayers, Stranski–Krastanov model, has not considered the overlapping between layers. We believe that a second layer of deposit starts to grow prior to the completion of the first layer.

The values of the characteristic parameters, $A_iN_{0i}k_i^2$, etc. are obtained through the best fit into the experimental current transient and presented in Table 1. According to this table, all kinetic parameters of nucleation and growth increase with increasing applied cathodic potential. At more cathodic potentials, however, the kinetic parameters of the third layer decrease and its contribution in nucleation and growth decreases (Fig. 5b). Decreasing $A_iN_{0i}k_i^2$ value may be partly due to the rapid formation of a not-properly-crystallized first and second layer, which might not provide a sufficient number of sites required for the third layer formation and lead to the start of 3D nucleation and growth very soon. Therefore, nucleation on upper layers becomes less significant as the deposition potential is made more cathodic. Table 1 also presents the double layer charging rate parameters presented as k_{D1} and k_{D2} in the first term of the left-hand side of Eq. (13). From these parameters, double layer capacitance can be obtained $C_{dl}=1.3\times10^{-3}$ F cm^{-2} with assumption $k_{D1}=E/R_s$ and $k_{D2}=1/R_sC_{dl}$ [49], with R_s and C_{dl} are solution resistance and double layer capacitance. These values have also been obtained through the fitting procedure.

Conclusion

Electrodeposition of palladium onto a stainless steel electrode from 0.04 M $Pd(NH_3)_4Cl_2$, NH_4Cl, and NH_4OH bath as studied by the methods of cyclic voltammetry, chronopotentiometry, and chronoamperometry revealed that electrodeposition of palladium proceeds via nucleation and growth mechanism. Potential transient indicates that palladium reduction is not diffusion controlled and Sand's law is not obeyed. Chronoamperograms revealed that the electrodeposition at applied cathodic potentials proceeds via 2D instantaneous nucleation followed by a multitude of

Table 1 Kinetic parameters obtained from the non-linear fitting of Eq. (13) to the potentiostatic current transients shown in Fig. 4

E (V/Ag–AgCl)	$N_{01}k_1^{2}{}_{(2DI)}$ (mol^2 cm^{-6} s^{-2})	$A_1N_{02}k_2^{2}{}_{(2DP)}$ (mol^2 cm^{-6} s^{-3})	$A_2N_{03}k_3^{2}{}_{(2DP)}$ (mol^2 cm^{-6} s^{-3})	$k_{2g(3D)}\times10^7$ (mol cm^{-2} s^2)	$A_gN_{0g}k_{1g}^{2}{}_{(3D)}$ (mol^2 cm^{-6} s^{-3})	$k_{1\ (DL)}$ (A cm^{-2})	$k_{2\ (DL)}$ (s^{-1})
−0.79	0.0117	0.0206	0.0127	1.03	0.0498	0.006	7.5
−0.8	0.0121	0.0218	0.0139	1.22	0.0546	0.007	7.4
−0.81	0.0141	0.0279	0.0279	1.36	0.0571	0.0075	7.8
−0.82	0.0162	0.0352	0.0511	1.43	0.0648	0.008	8
−0.83	0.0263	0.0851	0.0486	1.81	0.0651	0.0091	8.2
−0.84	0.0453	0.0923	0.0449	2.03	0.0668	0.0105	8.2

progressive nucleation and growth with considerable and determining overlap between the aforementioned steps. The phenomena are manifested as broad maxima on decaying amperograms. The current transient terminates to a plateau due to 3D nucleation and growth. The magnitudes of the kinetic parameters associated with each step and the parameter reflecting double layer charging in the initial stages of deposition have been reported.

References

1. Hjuler HA, Berg RW, Bjerrum NJ (1985) J Power Sources 10:1
2. Beratazzoli R, Pletcher D (1993) Electrochim Acta 38:671. doi:10.1016/0013-4686(93)80237-T
3. Gomez E, Marin M, Sanz F, Valles E (1997) J Electroanal Chem 422:139. doi:10.1016/S0022-0728(96)04899-1
4. Cruz MS, Alanzo F, Palacois JM (1993) J Appl Electrochem 23:364. doi:10.1007/BF00296693
5. Souteyrard E, Maruin G, Merciner D (1984) J Electroanal Chem 161:17. doi:10.1016/S0022-0728(84)80246-6
6. Gunawardena G, Hills G, Montenegro I, Scharifker B (1982) J Electroanal Chem 138:225. doi:10.1016/0022-0728(82)85080-8
7. Astely DJ, Harrison JA, Thirsk HR (1968) Trans Faraday Soc 64:192. doi:10.1039/tf9686400192
8. Fleischmann M, Thirsk HR (1960) Electrochim Acta 2:22. doi:10.1016/0013-4686(60)87005-3
9. Gunawardena GA, Hills GJ, Montenegro I (1978) Electrochim Acta 23:693. doi:10.1016/0013-4686(78)80026-7
10. Fleischmann M, Thirsk HR (1963) In Delahay P (ed), Advanced electrochemistry and electrochemical engineering, vol. 3. Academic, New York, pp 123
11. Volmer O (1926) Z Phys Chem 119:277
12. Gruz TE, Volmer M (1931) Z Phys Chem Abt A157:165
13. Somorjai GA (1994) Surface chemistry and catalysis. Wiley, New York
14. Rodriguez JA (1996) Surf Sci Rep 24:223. doi:10.1016/0167-5729(96)00004-0
15. Llorca MJ, Feliu JM, Aldaz A, Clavilier J (1994) J Electroanal Chem 376:151. doi:10.1016/0022-0728(94)03506-7
16. Gomez R, Rodes A, Perez JM, Feliu JM, Aldaz A (1995) Surf Sci 327:202. doi:10.1016/0039-6028(94)00832-9
17. Baldauf M, Kolb DM (1996) J Phys Chem 100:11375. doi:10.1021/jp952859m
18. Naohara H, Ye S, Uosaki K (2000) Electrochim Acta 45:3305. doi:10.1016/S0013-4686(00)00440-0
19. Naohara H, Ye S, Uosaki K (2001) J Electroanal Chem 500:435. doi:10.1016/S0022-0728(00)00390-9
20. Chen SC, Tu GC, Hung CCY, Huang CA, Rei MH (2008) J Membr Sci 314:5. doi:10.1016/j.memsci.2007.12.066
21. Harrison JA, Sierra A, Icazer HB, Thompson J (1974) J Electroanal Chem 53:145. doi:10.1016/0022-0728(74)80010-0
22. Crosby JN, Harrison JA, Whitfield TA (1981) Electrochim Acta 26:1647. doi:10.1016/0013-4686(81)85140-7
23. Corduneanu O, Diculescu VC, Chiorcea-Paquim AM, Oliveira-Brett AM (2008) J Electroanal Chem 624:97. doi:10.1016/j.jelechem.2008.07.034
24. Mourato A, Correia JP, Siegenthaler H, Abrantes LM (2007) Electrochim Acta 53:664
25. Quayum ME, Ye S, Uosaki K (2002) J Electroanal Chem 520:126
26. Hinch BJ, Koziol C, Toennies JP, Zhang G (1991) Vacuum 42:309. doi:10.1016/0042-207X(91)90043-I
27. Meyer G, Michailov M, Henzler M (1988) Surf Sci 202:125. doi:10.1016/0039-6028(88)90065-9
28. Baldauf M, Kolb DM (1993) Electrochim Acta 38:2145. doi:10.1016/0013-4686(93)80091-D
29. Pawar SM, Moholkar AV, Shinde PS, Rajpure KY, Bhosale CH (2008) J Alloy Comp 459:515. doi:10.1016/j.jallcom.2007.05.015
30. Vazquez-Arenas J, Cruz R, Mendoza-Huizar LH (2006) Electrochim Acta 52:892. doi:10.1016/j.electacta.2006.06.022
31. Gomes A, da Silva Pereira MI (2006) Electrochim Acta 51:1342. doi:10.1016/j.electacta.2005.06.023
32. Kubisztal J, Budniok A (2008) Int J Hydrogen Energy 33:4488. doi:10.1016/j.ijhydene.2008.06.023
33. Kubisztal J, Budniok A (2006) Appl Surf Sci 252:8605. doi:10.1016/j.apsusc.2005.11.074
34. Han Q, Li X, Chen J, Liu K, Dong X, Wei X (2005) J Alloy Comp 400:265. doi:10.1016/j.jallcom.2005.04.020
35. Duncan H, Lasia A (2008) Electrochim Acta 53:6845. doi:10.1016/j.electacta.2007.12.012
36. Fletcher S (1983) Electrochim Acta 28:917. doi:10.1016/0013-4686(83)85167-6
37. Fletcher S, Halliday CS, Gates D, Westcott M, Lwin T, Nelson G (1983) J Electroanal Chem 159:267. doi:10.1016/S0022-0728(83)80627-5
38. Salinas DR, Cobo EO, Garcia SG, Bessone JB (1999) J Electroanal Chem 470:120. doi:10.1016/S0022-0728(99)00220-X
39. Jafarian M, Mahjani MG, Gobal F, Danaee I (2006) J Appl Electrochem 36:1169. doi:10.1007/s10800-006-9192-1
40. Jafarian M, Gobal F, Danaee I, Mahjani MG (2007) Electrochim Acta 52:5437. doi:10.1016/j.electacta.2007.02.068
41. Hills DJ, Schriffrin DJ, Thomson J (1974) Electrochim Acta 19:657. doi:10.1016/0013-4686(74)80008-3
42. Lantelme F, Chevalet J (1981) J Electroanal Chem 121:311
43. Gunawardena G, Hills G, Montenegro I, Scharifker B (1982) J Electroanal Chem 138:225. doi:10.1016/0022-0728(82)85080-8
44. Stafford GR, Haarberg GM (1999) Plasma Ions 2:35. doi:10.1016/S1288-3255(99)80010-0
45. Barradas RG, Bosco E (1985) J Electroanal Chem 193:23. doi:10.1016/0022-0728(85)85049-X
46. Bewick A, Fleischmann M, Thirsk HR (1962) Trans Faraday Soc 58:2200. doi:10.1039/tf9625802200
47. Armstrong RD, Fleischmann M, Thirsk HR (1966) J Electroanal Chem 11:208. doi:10.1016/0022-0728(66)80083-9
48. Lorenz WJ, Staikov G (1995) Surf Sci 335:32. doi:10.1016/0039-6028(95)00576-5
49. Bard AJ, Faulkner LR (2001) Electrochemical methods. Wiley, New York